Preliminary modelling of power losses in roller chain drive: application to single speed cycling

Gabriel Lanaspeze, Bérengère Guilbert, Lionel Manin, Fabrice Ville

Mechanics & Industry **23**, 27 (2022)

https://doi.org/10.1051/meca/2022026

Mechanics & Industry

Available online at:
www.mechanics-industry.org

REGULAR ARTICLE

OPEN ACCESS

Preliminary modelling of power losses in roller chain drive: application to single speed cycling

Gabriel Lanaspeze, Bérengère Guilbert*, Lionel Manin, and Fabrice Ville

Univ Lyon, INSA Lyon, CNRS, LaMCoS, UMR5259, 69621 Villeurbanne, France

Received: 11 May 2022 / Accepted: 24 September 2022

Abstract. A quasi-static chain drive model is proposed. This model, consistent with single speed cycling application, applies to simple two sprocket drives. The kinematics of the transmission is determined, including the capture and release positions of the rollers and the influence of the polygonal effect. The tensions into the links and the contact forces (between rollers and sprocket) are then calculated based on the results of the kinematic analysis. Both chain strands are assumed to be straight and their tension are considered as imposed. An estimate of the roller displacement is proposed using existing studies on the relationship between loading conditions and roller positions along the sprocket tooth profile. The presented model, is then used to assess the contribution of both meshing and roller motion on the global efficiency of the drive. Calculations show that the magnitude of both loss sources is similar for a wide range of gear ratios and loading conditions. According to the presented results, the relative motion between the rollers and the sprocket tooth profile should be considered in future studies dedicated to chain drive efficiency.

Keywords: Roller chain / kinematics / load calculation / efficiency / roller motion

1 Introduction

Modern roller chains were introduced by Hans Renold in the late 19th century. Since then, they have widely been used in mechanical applications, from handling to internal combustion engines [1–3]. They are also used in bicycle drives in order to transmit power from the pedals to the rear wheel.

Although chain drives are known for their high energetic efficiency (about 99% for single speed transmissions, [4,5]), several studies have been presented to explain the phenomena responsible for power losses [4–9]. Among these works, different potential sources of dissipation have been considered.

Meshing losses have been the subject of most studies in this field. These losses are caused by a rotational movement experienced by each link when it is captured or released by a sprocket (Fig. 1). This phenomenon is assumed to be preponderant in [7] on power losses in heavy cranked link chain. With the same hypothesis, Lodge and Burgess [4] presented efficiency predictions for simple two-sprocket drive using a new model for link tension and contact force calculation.

Work by Spicer et al. [6], Kidd [5], and Zhang and Tak [9] focused on bicycle transmissions. They evaluate the influence of derailleur and offset conditions on the performance. However, these effects should be negligible for single speed applications.

Chain drive are also subjected to strand vibrations. An experimental example can be found in [10]. The first effort to model this phenomenon was by Binder [11]. Further works considering the chain strands as a uniform string with moving boundary conditions have been conducted in [12,13]. Impacts are also known to occur between the rollers and the sprockets, with a significant influence on the drive noise. An experimental observation of this phenomenon is presented in [14]. First modelling attempts can be found in [11,15]. These phenomena (i.e. vibration and roller impacts) are very complex and their influence, in term of power losses, is still unquantified. Possible non-linearities in the elastic behaviour of the links have also been explored by Spicer [8] and could be responsible for limitation of efficiency.

Finally, studies have also been presented on the motion of rollers along their corresponding tooth profile (Fig. 1). A first approach on this subject can be found in [11]. Naji and Marshek extended the analysis to evaluate the influence of chain elongation on chain-sprocket interactions [16,17]. Later, Kim and Johnson [18] and Troedsson and Vedmar [19] studied the influence of loading conditions on the relative position between each roller and its corresponding tooth profile. However, the influence of the induced roller motion on efficiency have not yet been investigated.

* e-mail: berengere.guilbert@insa-lyon.fr

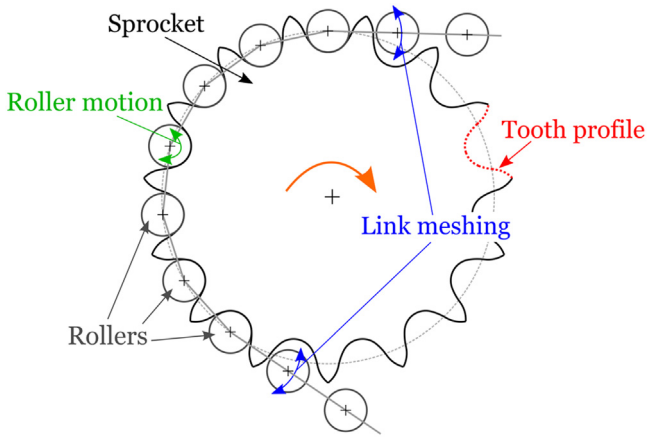

Fig. 1. Meshing and roller motion on a sprocket.

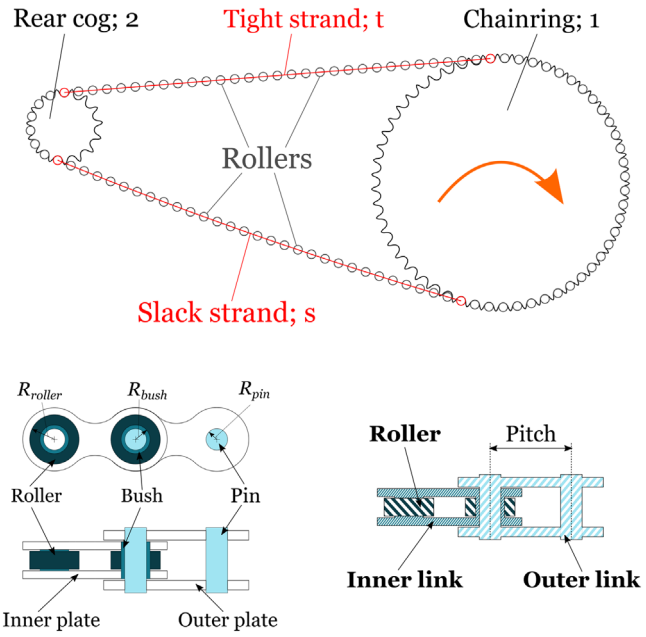

Fig. 2. Vocabulary for cycling chain drive.

This paper focuses on losses due to friction between parts (i.e. meshing and roller motion losses). The aim is to estimate the contribution of each phenomenon to the transmission efficiency.

First, a quasi-static model dedicated to two sprocket drive is presented. The kinematics of the transmission is determined using a new numerical procedure. The geometrical fluctuations caused by the polygonal shape of a chain wrapping on a given sprocket (i.e. polygonal effect [20]) are considered. The loads (link tension and roller/sprocket contact force) are calculated from the kinematics using the existing tension model presented by Lodge [4]. Both the tight and slack strand are assumed to be straight.

The resulting drive model is then used to estimate the contribution of each power loss source. The contribution of the roller motion is compared to the magnitude of meshing losses to determine the relative influence of this dissipation source on the global transmission efficiency.

This study focuses on single speed cycling application (bicycle drive with no derailleur system). In this type of chain drive, the driver sprocket is called chainring and the driven sprocket is called rear cog (respectively denoted 1 and 2). The tight and slack strands of the drive are respectively denoted t and s.

A typical single speed drive is represented in Figure 2 along with a schematic of chain.

2 Chain drive model

The presented model assumes that all bodies are rigid. This includes the tight and the slack strands considered as one straight body each. This hypothesis is not very restrictive in the context of single speed cycling as the drives are usually set with non-negligible tension in the slack strand which significantly constrains its trajectory. Moreover, as bicycle chains are usually relatively light (≈3.5 g/link), and with low rotational speed (150 rpm on the chainring at most), dynamic effects are considered negligible. Thus, the presented model is quasi-static, and is therefore not subject to any speed or inertia effects. Both sprockets are assumed to be perfectly aligned and their pitch are identical to the chain pitch (denote p). The kinematics is considered independent from the loads and only the global motions of the bodies are modelled. Therefore, backlashes, as well as relative motions between each roller and its corresponding tooth profile are neglected. Consequently, the centre of every roller in contact with a sprocket is assumed to lie on the pitch circle (Fig. 3). Finally, the effect of gravitation is also neglected with regard to the loads involved.

The transmission behaviour of the resulting model is cyclic. Its angular period corresponds to a rotation of both sprockets by their respective angular pitch (α_1 on the chainring and α_2 on the rear cog, see Fig. 3).

The modelling strategy is divided into two main steps. First, the drive kinematics is established (i.e. the location of each components) for a given set of drive positions. Then, loads are calculated depending on the determined locations.

2.1 Chain drive kinematics

2.1.1 Kinematic parameters

According to [15], the basics of chain drive geometry is defined in Figure 3 using the following parameters.

- $L = [O_1O_2]$, the centre distance between the chainring and rear cog.
- $\alpha_j = 2\pi/Z_j$, the tooth angle for sprocket j (Z_j stands for the number of teeth).
- $\alpha_{t,1}$ ($\alpha_{t,2}$), the angle between the tight strand and the closest link with both rollers contacting the chainring (rear cog).
- $R_j = p/[2\sin(\alpha_j/2)]$, the pitch circle radius.

Index j designates a specific sprocket (1 for the chainring, 2 for the rear cog).

The direction of the common tangent to both pitch circles is given by the angle β and the two tangency points are M_1 on the chainring and M_2 on the rear cog, see Figure 3a.

$$\beta = \sin^{-1}\left(\frac{R_1 - R_2}{L}\right) \tag{1}$$

The tight strand tips are defined geometrically as the centres of the first and last roller in contact with the chainring and the rear cog respectively. As the strand is considered straight, articulation between links only occur at these points.

The strand tips positions vary during the transmission operation. Therefore, the direction of the tight strand is distinct from the direction of the common tangent. To account for these variations, the following angles are introduced:

– Angle β_t measures the tight strand direction (relatively to direction O_1O_2).
– Angles $\psi_{t,j}$ track the strand tip positions (measured relatively to the tangency points M_j).

Figure 4 gives the definition of β_t and $\psi_{t,1}$ for the chainring. $\psi_{t,2}$ is defined in a similar way on the rear cog.

Yet, angles $\psi_{t,1}$ and $\psi_{t,2}$ are not independent variables as the tight strand induces a relationship between the rotations of the chainring and rear cog. This dependence can be modelled using a four-bar mechanism (Fig. 5) [20,21].

Developing the chain closure condition leads to the following equations:

$$\begin{cases} x_t \sin(\beta_t) + R_2 \cos(\psi_{t,2} + \beta) - R_1 \cos(\beta - \psi_{t,1}) = 0 \\ x_t \cos(\beta_t) - R_2 \sin(\psi_{t,2} + \beta) + R_1 \sin(\beta - \psi_{t,1}) = L \end{cases} \tag{2}$$

with:

$$x_t = n_t.p, \tag{3}$$

n_t being the number of links into the tight strand.

The resulting system of equations consists of four variables ($\psi_{t,1}$, $\psi_{t,2}$, β_t, and x_t) and two equations.

For the tight strand, β_t and $\psi_{t,2}$ are computed from $\psi_{t,1}$ and x_t using a Newton-Raphson algorithm.

Once both strand tip positions are known (i.e. angles $\psi_{t,j}$), the corresponding values for the angles $\alpha_{t,j}$ are obtained.

The equation for $\alpha_{t,1}$ is given below (using Fig. 6). Similar equations can be obtained for $\alpha_{t,2}$.

$$\alpha_{t,1} = \beta_t - \theta \tag{4}$$

with:

$$\begin{cases} \cos(\theta) = \dfrac{R_1[\sin(\beta - \psi_{t,1}) - \sin(\beta - \psi_{t,1} - \alpha_1)]}{p} \\ \sin(\theta) = \dfrac{R_1[\cos(\beta - \psi_{t,1} - \alpha_1) - \cos(\beta - \psi_{t,1})]}{p} \end{cases} \tag{5}$$

Expressions for θ are obtained considering the scalar product of the vector $\vec{c_1c_2}$ with $\vec{x}$ and $\vec{y}$.

The specific values of $\alpha_{t,j}$ allow to characterise remarkable drive positions. Indeed, the strand tip position (Fig. 7) moves along the pitch circle during transmission operation. Figure 7 illustrates the two extreme tight strand tip positions (for the chainring). In Figure 7a, the chainring orientation is such that roller B just makes contact (i.e. the roller B is captured). At this specific moment, the angle $\alpha_{t,1}$ is 0^+. On the contrary, in Figure 7b, the chainring is positioned right before the capture of a new roller from the tight strand (roller A), and $\alpha_{t,1} = \alpha_1$. The tight strand tip then jumps to roller A and the movement starts over.

Hence, for any chainring orientation, the values of $\alpha_{t,1}$ are restricted to $[0, \alpha_1]$. Similarly, the values of $\alpha_{t,2}$ are restricted to $[0, \alpha_2]$, and the rear cog position where $\alpha_{t,2} = \alpha_2$ marks the release of a new roller into the tight strand.

Finally, the slack strand is modelled as the tight one. Hence, parameters $\alpha_{s,j}$, $\psi_{s,j}$, β_s and x_s are defined by a similar method as, respectively, $\alpha_{t,j}$, $\psi_{t,j}$ β_t and x_t. Therefore, the dependencies detailed above for the tight strand parameters are also valid for the slack ones.

However, the slack and tight strand tip positions are intertwined as the angles $\psi_{t,j}$ and $\psi_{s,j}$ are related by equation (6).

$$\pi - 2 \times (-1)^j \beta = \psi_{t,j} + \alpha_j n_j + \psi_{s,j} \tag{6}$$

with n_j the number of links with both rollers contacting sprocket j ($j = 1$ or 2 for the chainring and the rear cog respectively).

2.1.2. Computation procedure

This section details the computation procedure used to determine the positions of all the chain parts (i.e. the kinematics of the drive).

The initial chainring orientation is given by the angle $\psi_{t,1,init}$.

The transmission motion is discretised into a number of chainring orientations and the numerical procedure detailed hereafter is used separately for each.

First, the geometry of the tight strand (i.e. angles $\alpha_{t,j}$, $\psi_{t,j}$, β_t, and n_t) is computed using the algorithm given in Figure 8.

The algorithm is initialized for $\psi_{t,1}$ and n_t.Values are predicted based on the global geometrical characteristics of the drive (distance L, number of teeth Z_j, etc.). Then, $\psi_{t,2}$ and β_t are calculated using equation (2). Finally, the induced angles $\alpha_{t,1}$ and $\alpha_{t,2}$ are calculated from equation (4) and are compared with the interval $[0,\alpha_j]$. If their values lie outside the interval, the initial predictions are modified accordingly until an acceptable configuration is found.

The slack strand is then solved using the algorithm from Figure 9.

The general principle is the same, but the initial parameters differ. Indeed, for the tight strand, $\psi_{t,1}$ and x_t are predicted while $\psi_{t,2}$ and β_t are calculated from equation (2). Yet, for the slack strand, the numbers of links n_1 and n_2 are the initialization variables. Their values directly constrain $\psi_{s,1}$ and $\psi_{s,2}$ *via* equation (6). Then, as for the tight strand, β_s, x_s and $\alpha_{s,j}$ are calculated using equations (2) and (4) before the obtained value for $\alpha_{s,j}$ are

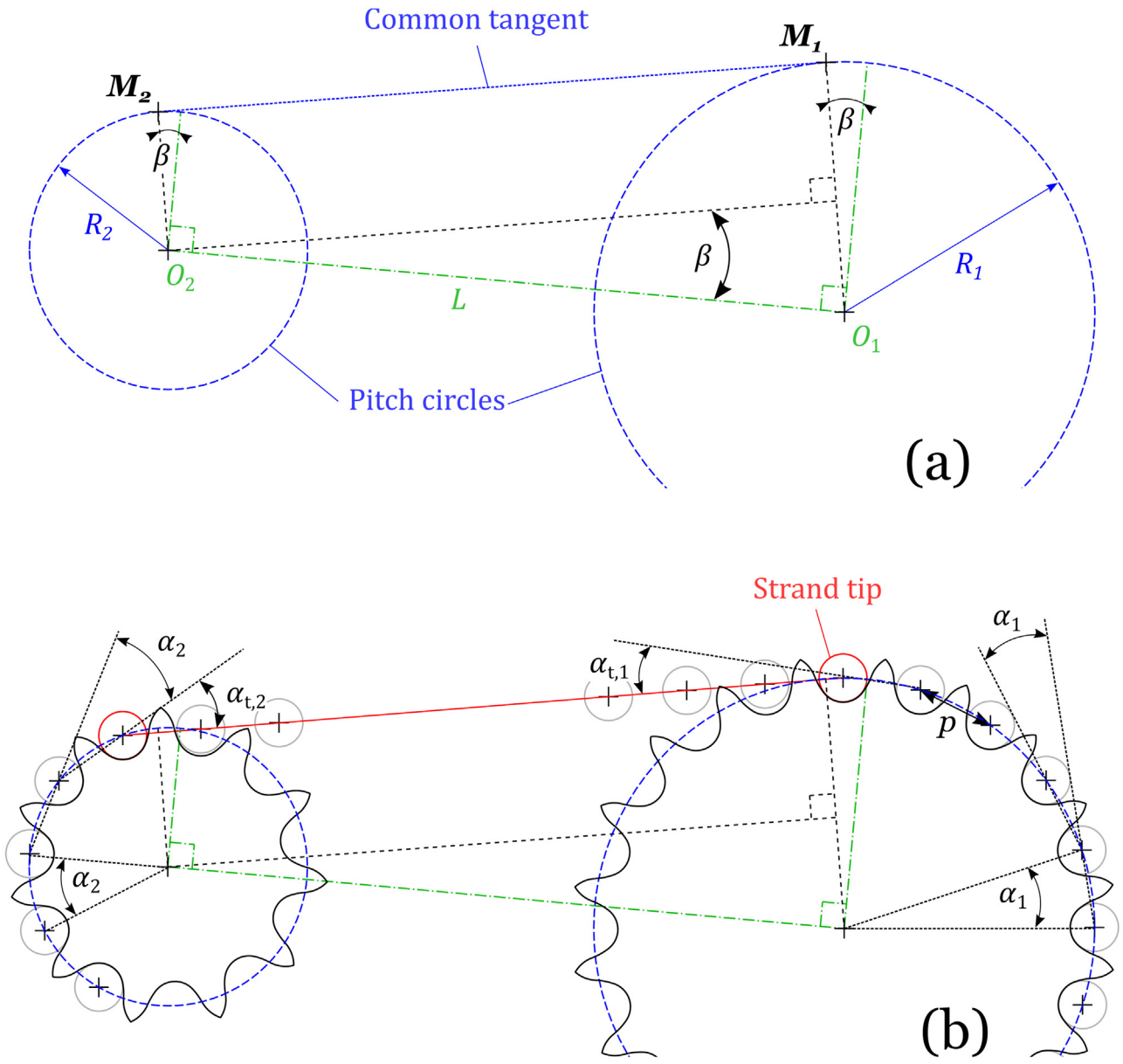

Fig. 3. Basic definition of chain drive geometry.

compared to the interval $]0, \alpha_j]$. In the same way as the tight strand, if angles $\alpha_{s,j}$ lie outside $]0, \alpha_j]$, the predictions on n_j are changed.

Due to the construction of the model, the slack strand tip positions are fully constrained by the tight strand and the numbers of links n_1 and n_2. Therefore, the length of the slack strand x_s cannot be exactly a multiple of the chain pitch, as it would be in reality. It is then assumed that the slack strand can withstand little variations of x_s. In practice, the distance L between sprockets (Fig. 5) is chosen so that the ratio x_s/p is very close to an integer (details will be given in Sect. 3.2).

For all tested drive configurations, the solution obtained with the given procedure was unique and independent from the starting predictions.

2.2 Load calculation

The kinematic parameters are now used to calculate the loads in the drive.

For this purpose, the tension model presented by Lodge and Burgess [4] is used. This model is a synthesis of previous work by Binder [11] and Naji and Marshek [22,23] as well as new features, specific to cases where slack strand tension is low. It allows the calculation of the tension forces T_i in each link as well as the contact forces P_i between each roller and its corresponding contacting sprocket. The tension forces in both the tight and slack strand (respectively T_t and T_s) are assumed to be known (relation between tensions and torque apply on a sprocket is given in Sect. 3.1.2).

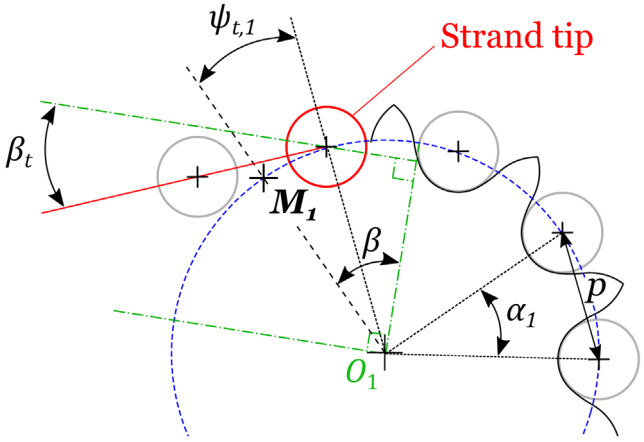

Fig. 4. Definition of $\psi_{t,1}$ and β_t.

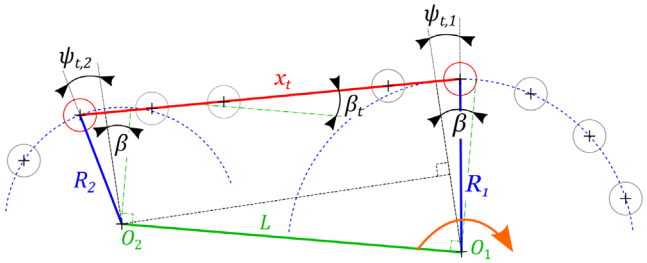

Fig. 5. Four-bar modelling of the tight strand.

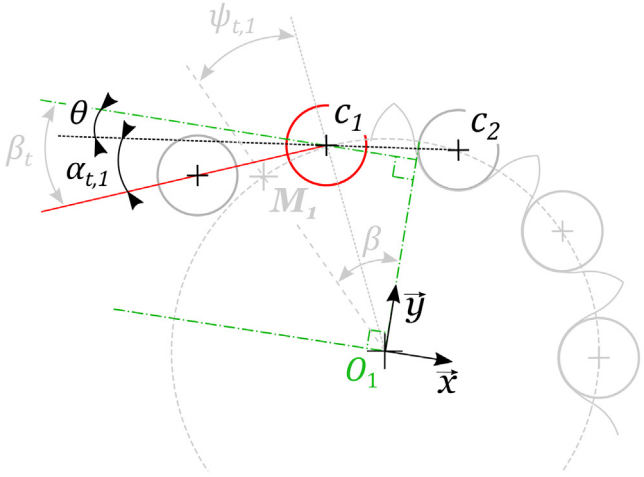

Fig. 6. Calculation of $\alpha_{t,1}$.

For each roller in contact with a given sprocket, the equilibrium of the corresponding articulation (i.e. set of pin, bush and roller, see Fig. 2) is considered. Thus, each articulation is subjected to only three external forces:
– The tension forces in the previous and in the following link (respectively T_i and T_{i+1}).
– The contact force between the roller and the sprocket P_i.

In addition, it is assumed that a roller has only three possible positions along its corresponding tooth profile. The main difference between these three possibilities being the value of the angle ϕ (call pressure angle). This angle is defined between the direction of P_i and either T_i or T_{i+1} depending on the roller position (see Fig. 10).

For the first two cases, the roller is seated (i.e. at the bottom of the tooth profile), and can contact either the slack or the tight side of the profile, respectively (a) and (b) in Figure 10. For both seated positions, the point of contact (either on the tight side or on the slack side) is such that the pressure angle ϕ is equal to the value given in the standards [11,18]. This value is only valid for the ASA profile. For the third case, it is assumed that the roller climbs the tight side of the tooth profile (see (c) in Fig. 10). In this position, the pressure angle is set to ϕ_{min} [11,18].

No intermediate locations are possible and all the transitions are assumed to be instantaneous.

Moreover, the variations in the positions of the rollers along their tooth profile are considered small compared to the global transmission kinematics determined previously. Thus, the roller centres are still assumed to be on the pitch circle, and the angle between the direction of two consecutive links, with both rollers in contact with the sprocket, is always α (i.e. the angles between directions T_i and T_{i+1}).

Furthermore, the model assumes that sliding occurs at the contacts between rollers and sprocket. Therefore, neglecting the moment at the roller centre, friction is introduced using the angle $\delta = \text{atan}(\mu)$, μ being the friction coefficient at the roller/tooth contact. This angle is used to correct the value of the pressure angle ϕ. The sign of the correction ($\pm\delta$) is related to the direction of the friction force F_i (Fig. 11). This force opposes the movement of the roller along its corresponding tooth profile. Its direction depends on the considered sprocket (chainring or rear cog), and on the roller position along its tooth profile (in contact with the tight or slack side). This method was first proposed by Naji and Marshek [22].

In the following developments, the sign of δ is taken for a driven sprocket (rear cog). The equations for the chainring can be obtained by reversing this sign.

For all the equations detailed in this section, α, α_s, α_t, and n stand respectively for α_j, $\alpha_{s,j}$, $\alpha_{t,j}$, and n_j, as defined in Section 2.1.

Forces acting on an articulation with roller contacting the tight side of its tooth profile are represented in Figure 11. It is assumed that all the forces are concurrent at the roller centre (the moment induced by friction is neglected [22]). The equilibrium of the articulation leads to the following equations (details are given in Appendix A):

$$\begin{cases} T_{i+1} = T_i \dfrac{\sin(\phi - \delta)}{\sin(\phi - \delta + \alpha)} \\ P_i = T_i \dfrac{\sin(\alpha)}{\sin(\phi - \delta + \alpha)} \end{cases} \tag{7}$$

Using symmetry considerations, the equations between T_i, T_{i+1} and P_i for articulations with roller in contact with the slack side are obtained by reversing the sign of δ and swapping T_i and T_{i+1} in the equations (7).

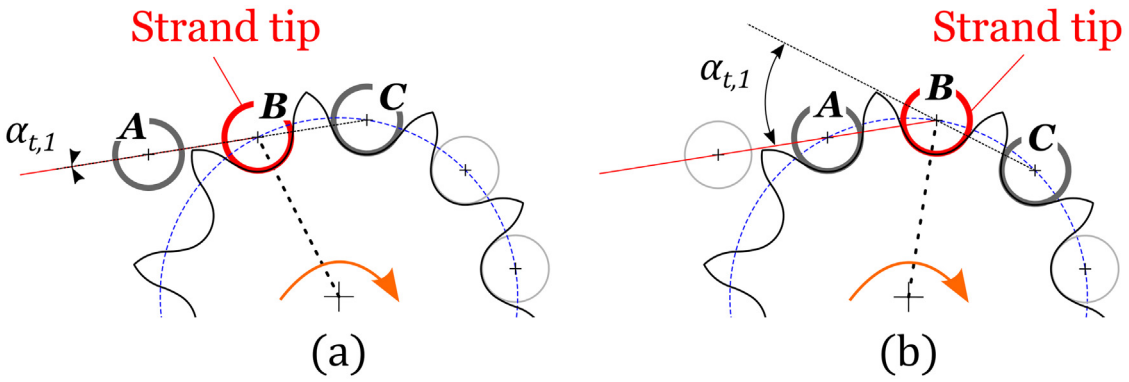

Fig. 7. Extreme positions for the tight strand tip on the chainring $\alpha_{t,1} = 0^+$ for (a) and $\alpha_{t,1} = \alpha_1$ for (b).

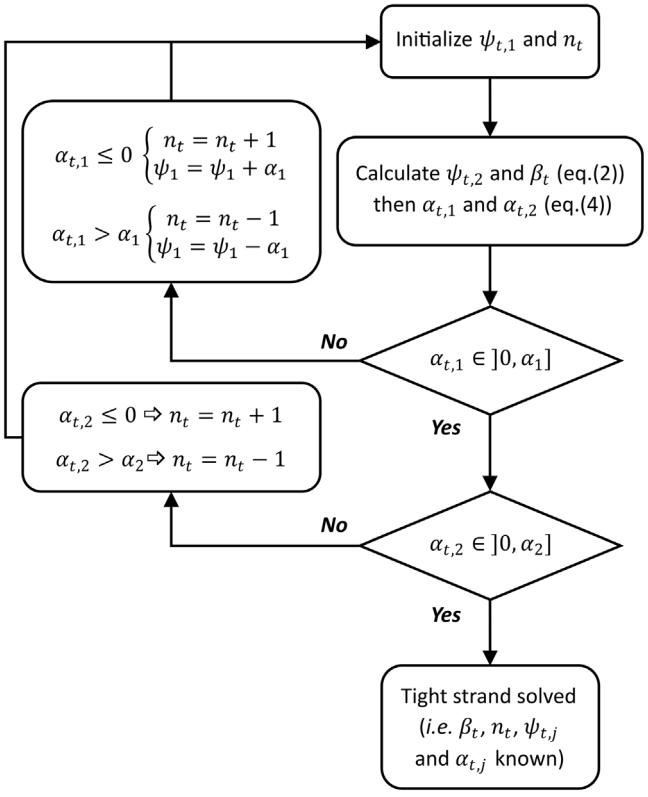

Fig. 8. Flow chart for the tight strand computation.

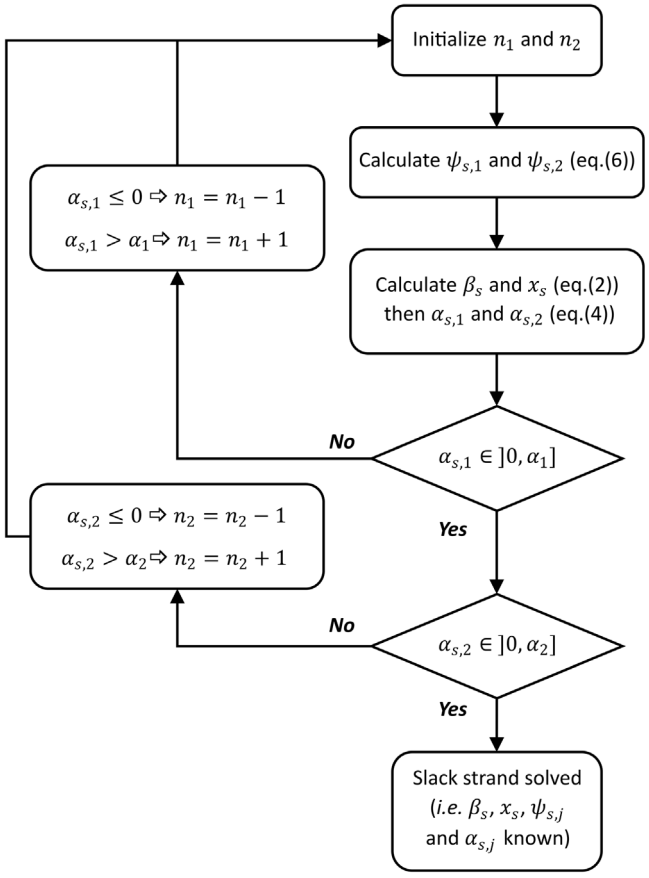

Fig. 9. Flow chart for the slack strand computation.

Lodge's model is composed of three sub-models [4,11,22,23]. The choice is made according to the tension ratio T_s/T_t. The Geometric Progressive Load Distribution (GPLD) sub-model is relevant for most real cases. Thus, only this one is described here.

In this sub-model, it is considered that the first rollers (as numbered in Fig. 12) are in contact with the tight side of their tooth profile. Conversely, those closer to the slack strand are in contact with the slack side of their profile. In both positions, the rollers are seated (Fig. 10) and the transition from tight to slack contact is assumed to be instantaneous, as mentioned above.

The first roller to come into contact with the slack side is called transition roller. Its position on the sprocket depends on the loading conditions.

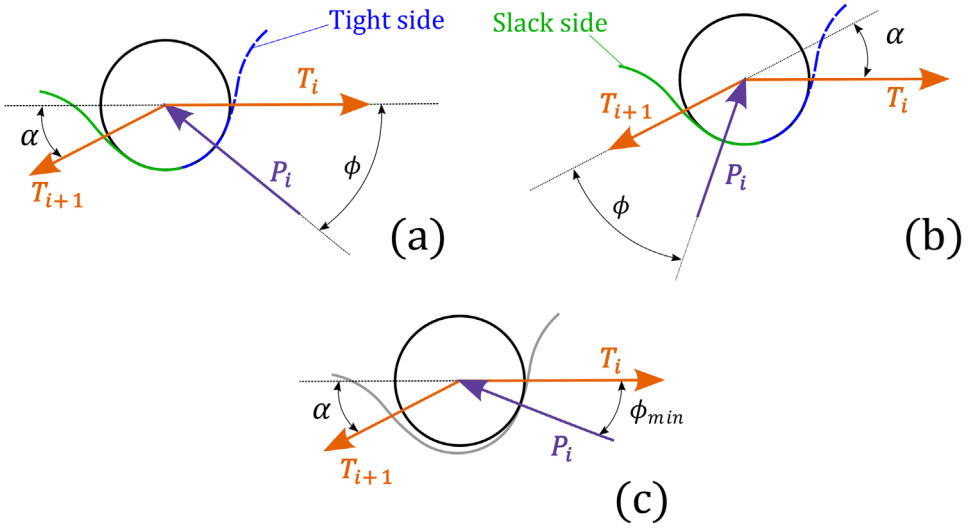

Fig. 10. Three possible roller positions in Lodge's model.

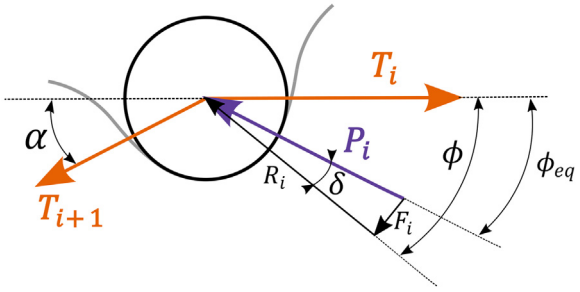

Fig. 11. Introduction of the friction angle δ.

Based on the link and roller numbering presented in Figure 12, $T_1 = T_t$ and $T_{n+2} = T_s$, n being the number of links with both rollers contacting the considered sprocket.

For the remaining links, those located before the transition roller (with rollers in contact with the tight side of their tooth profile) are considered first. Using equation (7), with q_- the ratio between T_{i+1} and T_i, gives:

$$T_{i+1} = T_t \frac{\sin(\phi - \delta + \alpha - \alpha_t)}{\sin(\phi - \delta + \alpha)} (q_-)^{(i-1)} \tag{8}$$

with:

$$q_- = \frac{\sin(\phi - \delta)}{\sin(\phi - \delta + \alpha)} \tag{9}$$

Similarly, for the links beyond the transition roller, including itself (i.e. roller in contact with the slack side of their tooth profile), the following equation is used:

$$T_{i+1} = T_s \frac{\sin(\phi + \delta + \alpha - \alpha_s)}{\sin(\phi + \delta + \alpha)} (q_+)^{(n-i)} \tag{10}$$

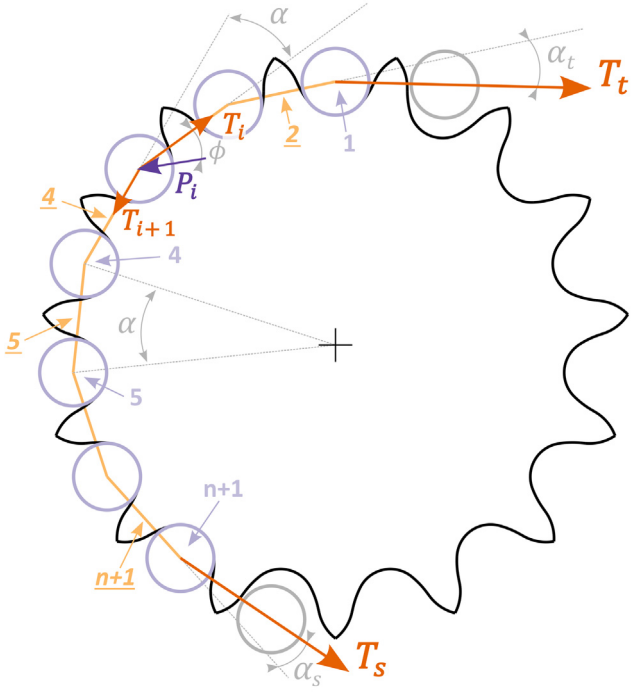

Fig. 12. Roller and link numbering.

with:

$$q_+ = \frac{\sin(\phi + \delta)}{\sin(\phi + \delta + \alpha)} \tag{11}$$

Finally, by combining the equations (8) and (10), the following expression for T_{i+1} is obtained ($i \in [1, n]$).

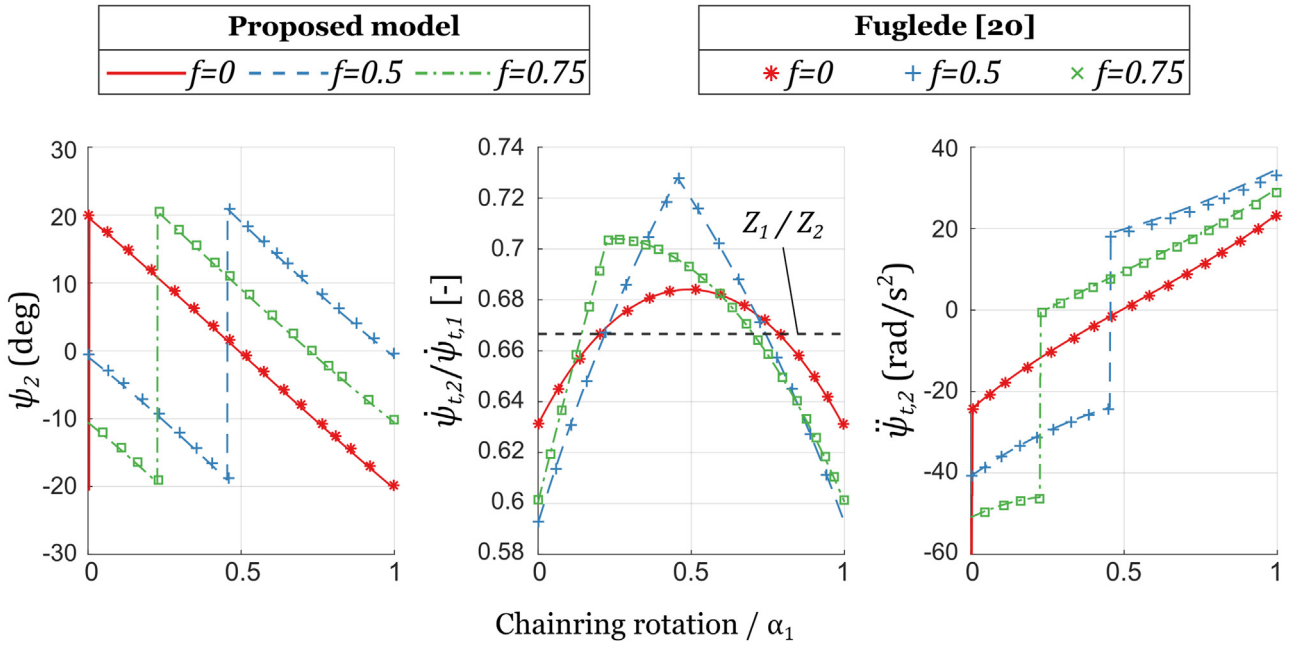

Fig. 13. Chain drive kinematics, comparison with Fuglede et al. [21].

See equation (12) below.

In equation (12), the two ratios of sine are related to the equilibrium of the first and last contacting rollers (i.e. rollers 1 and $n+1$ respectively). They are modified with respect to $q_{\pm}$ as angles α_t and α_s are distinct from α.

Once all the tensions T_i are known, values of P_i are obtained using equation (7).

As explained in Section 2.1, the angles α_t and α_s vary during one system period (i.e. chainring rotation of α_1). Consequently, equation (12) must be used for each sprocket position.

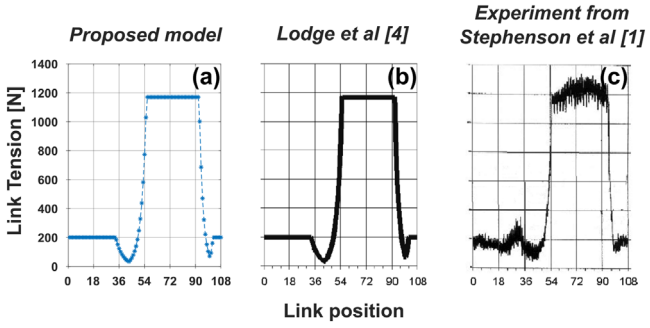

Fig. 14. Theorical and experimental link tension for a torque of 53 N m.

3 Preliminary calculations

3.1 Elements of validation

3.1.1 Chain drive kinematics

The procedure used for the kinematic calculation is compared to the results presented by Fuglede and Thomsen [21]. They studied particular drives where the sprocket arrangements are chosen such that the common tangent related to the tight strand is horizontal.

In [21], the considered number of teeth is $Z_1|Z_2 = 6|9$ (i.e. 6 teeth for the driver sprocket and 9 for the driven). Three different drives are studied, characterised by the value of the parameter f ($f = 0\,;0.5\,;0.75$). This parameter is defined as the rest of the Euclidian division between the length of the common tangent and the chain pitch, expressed as a fraction of the chain pitch. Therefore, f is related to the distance L by the following equation

$$L\cos(\beta) = (N+f)p \tag{13}$$

with:

$$\begin{cases} N \in \mathbb{N} \\ f \in [0,1] \end{cases} \tag{14}$$

The evolution of $\psi_{t,2}$, the angular velocity ratio $\dot{\psi}_{t,2}/\dot{\psi}_{t,1}$, and the rear cog angular acceleration $\ddot{\psi}_{t,2}$, are plotted in Figure 13, versus the chainring rotational angle (as a fraction of α_1). The instantaneous derivatives are

$$T_{i+1} = \max\left[T_t \frac{\sin(\phi-\delta+\alpha-\alpha_t)}{\sin(\phi-\delta+\alpha)}(q_-)^{(i-1)}; T_s \frac{\sin(\phi+\delta+\alpha-\alpha_s)}{\sin(\phi+\delta+\alpha)}(q_+)^{(n-i)}\right] \tag{12}$$

Table 1. Characteristics of the studied single speed transmission.

$Z_1 \vert Z_2$	T_s / T_t	L (mm)	Number of links	Pitch (mm)
60|15	0.1	386	100	12.7

computed numerically from the displacement between positions (obtained Sect. 2.1) using a central difference. The chainring angular velocity is set to 100 rpm.

The initial chainring orientations are such that a roller has just been captured by the chainring. The corresponding $\psi_{t,1,init}$ values are calculated as detailed in [21].

The two models are consistent for all tested variables. Remarkably, the roller capture and release positions (characterised by the discontinuities in the graphs) are well predicted.

The velocity transmission error ($\dot{\psi}_{t,2}/\dot{\psi}_{t,1}$) curves show that the velocity ratio between the chainring and the rear cog varies throughout a chainring period. This deviation is caused by the modification of the tight strand direction and is part of the polygonal effect. The highest velocity ratio deviation (compared to the theoretical value Z_1/Z_2) is obtained for $f = 0.5$. This configuration corresponds to cases where the instant of roller capture by the chainring and the instant of roller release by the rear cog occur in opposing phase.

The model is also consistent for drives with $Z_1|Z_2 = 12|18$ and 21|63 [21]. Thus, the procedure for kinematic calculation is validated for a wide range of chain drives (see Fig. B1 in Appendix B).

3.1.2 Loads computation

The loads predicted by the model are compared to the measurements presented by Stephenson et al. [1].

The drive configuration used for the experiments is $Z_1|Z_2 = 18|36$ and the chain pitch is $p = 9.525$ mm (3/8″). A torque $C = 53$ Nm is applied on the driver sprocket. Due to the specific application, a tensioner rail compels the slack strand tension at 200 N. Moreover, both strands trajectories are constrained by guide rails. Therefore, the procedure detailed in Section 2.1 for the chain drive kinematics cannot be used on this transmission. As a consequence, the chain drive model is modified in a similar way as in [4] to allow the comparison with the experiments. Thus, the number of links contacting each sprocket (n_j) are set with the values provided in [1], and the angles $\alpha_{t,j}$ and $\alpha_{s,j}$ are assumed to be constant and equal to $\alpha_j/2$. Due to these modifications, the geometric effects (e.g. polygonal effects) are not modelled.

In order to calculate the loads using the model from Lodge, the tight strand tension T_t must be known (see Sect. 2.2). It is calculated from the values of T_s and C (torque applied on the driver sprocket). Indeed, considering the equilibrium of the equivalence class constituted by the driver sprocket and all the links with both rollers in contact with it leads to the following relation between C, T_s and T_t.

$$C = R_j\left[T_t \cos\left(\alpha_{t,j} - \alpha_j/2\right) - T_s \cos\left(\alpha_{s,j} - \alpha_j/2\right)\right], \quad (15)$$

$$\Leftrightarrow T_t = \left[\frac{C}{R_j} + T_s \cos\left(\alpha_{s,j} - \alpha_j/2\right)\right] \times \frac{1}{\cos\left(\alpha_{t,j} - \alpha_j/2\right)} \quad (16)$$

with $j = 1$ for the driver sprocket (the relation can also be used for a driven sprocket provide that subscript j is set to 2).

Comparison of the obtained link tensions is presented in Figure 14. Tensions calculated with this model are on graph (a). Graphs (b) and (c) show the prediction of the original Lodge's model [4] and the experimental data from [1].

The links position on X-coordinate are set according to [1].

As expected, the agreement between (a) and (b) is very good. Despite the noise on the measurements, the correlation is also quite good with (c). The tension variation in the strands, noticed in the experimental data, is probably a consequence of the guide rails which are not considered in the model. Moreover, some of the high-frequency fluctuations might also be due to kinematic effects (e.g. variations in the value of angles $\alpha_{t,j}$ and $\alpha_{s,j}$) which are also neglected.

Based on this comparison, the loads computed using the chain drive model are considered valid and can therefore be used for loss calculations (Sect. 4).

3.2 Preliminary results

The parameters of the studied drive are presented in Table 1. They are chosen to be representative of a single speed transmission.

To characterise the load distribution, since no load-related effects (e.g. deformation of the parts) are taken into account, the definition of the tension ratio (T_s/T_t) is sufficient.

Using the procedure detailed in Section 2.1, the evolutions of n_j, $\alpha_{t,j}$ and $\alpha_{s,j}$ are computed over a chainring rotation of α_1. The results are shown in Figure 15. The starting position is taken at $\psi_{t,1,init} = 0$.

The discontinuities in the evolution of angles $\alpha_{t,j}$ and $\alpha_{s,j}$ are the manifestation of the capture/release of a roller by either one of the sprockets. The leap value is always α_1 for the chainring and α_2 for the rear cog. As these particular phenomena are generally not synchronised, the number of links in contact with a given sprocket (i.e. n_j) varies throughout a chainring angular period. The phase shift between these events depends on geometrical characteristics (distance L, total number of links, number of teeth Z_j, etc.). An appropriate choice of these parameters can lead to specific configurations where the captures and releases of rollers occur simultaneously.

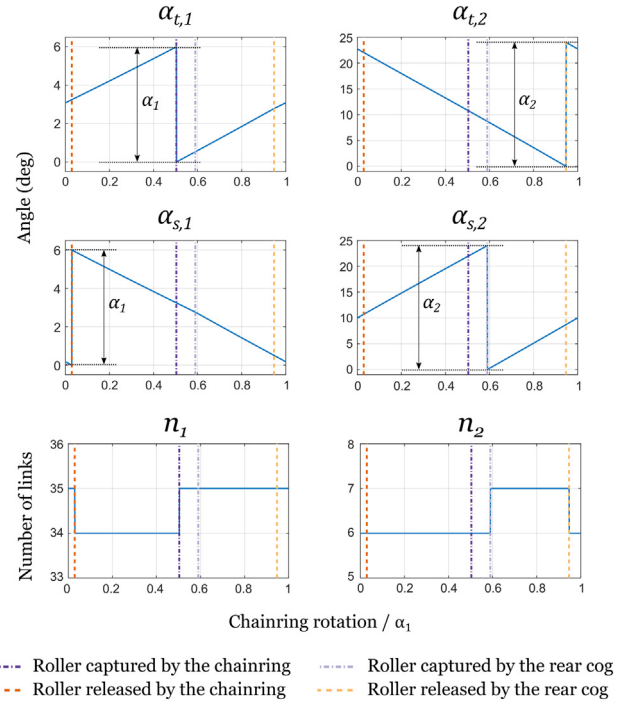

Fig. 15. Evolution of the main kinematic parameters for the 60|15 drive.

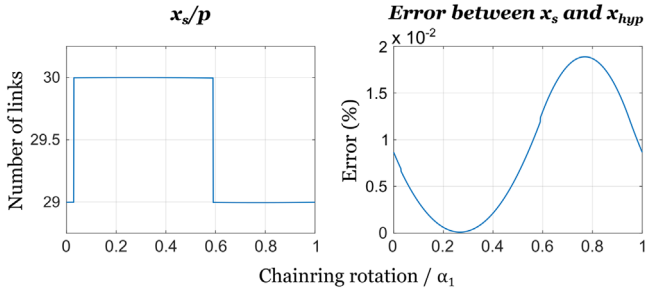

Fig. 16. Evolution of x_s/p.

As explained in Section 2.1, the length of the slack strand cannot be forced to equal a whole number of chain pitch. However, the distance L can be chosen so that the ratio x_s/p is numerically close to an integer (corresponding to drives where the assumption of straight slack strand is realistic). In the studied example, x_s is compared to the length of a hypothetical slack strand, x_{hyp} constituted of a number of links $n_s = \text{round}\,(x_s/p)$.

$$x_{hyp} = p.\,\text{round}(x_s/p) \tag{17}$$

Figure 16 shows that the error between the two lengths (with x_{hyp} as reference) is about 0.01%.

Using the presented values of n_j, $\alpha_{t,j}$ and $\alpha_{s,j}$ into the tension model gives the evolution of T_i and P_i for any drive positions.

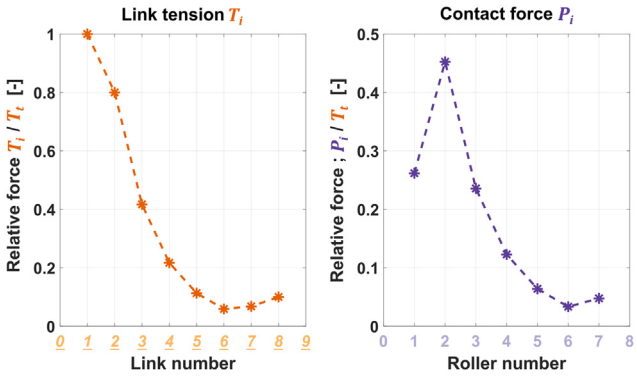

Fig. 17. Variation of $\boldsymbol{P_i}$ and $\boldsymbol{T_i}$ ($\boldsymbol{\psi_{t,1} = \alpha_1/2}$).

An example of load evolution for the rear cog is given in Figure 17. The rollers and links numbering on X-axis are as defined in Figure 12.

In the drive position of Figure 17, the transition roller (i.e. the first roller to contact the slack side of its tooth profile) is roller 7. As a consequence, the link tension first decreases up to link 6 (rollers in contact with the tight side of their profile). An increase is then observed until T_i reaches the slack strand tension ($T_s = 0.1\,T_t$ in this example).

The same behaviour is observed for the evolution of P_i. The contact force decreases until the transition roller and then increases again slightly. The first rise between rollers 1 and 2 is a consequence of the $\alpha_{t,2}$ value in this specific drive position ($\alpha_{t,2} \approx 0.45\alpha_2$ for this example). The main outcome being that the load is not evenly distributed among the teeth in contact with a roller.

The chain drive model has been shown able to calculate the kinematics and the load distribution for a given transmission. These results can now be used to compute the contribution of roller motion and link meshing to the overall transmission efficiency.

4 Estimation of the losses

4.1 Location of loss sources

The location of each loss source is presented in Figure 18. Meshing loss occurs each time a link is captured or released by a sprocket (chainring or rear cog). There is then a total of four meshing loss points (two for each sprocket). In addition, the dissipation due to roller motion occurs during the contact of each roller with the considered sprocket.

In order to compare the contribution of both type of losses, a single articulation between two links is considered (i.e. one pin, bush and roller). As this articulation travels its way throughout a full transmission rotation, it goes through the four meshing points and the two roller loss zones. The full dissipation caused by this articulation is then calculated as the sum of the contribution in all loss locations.

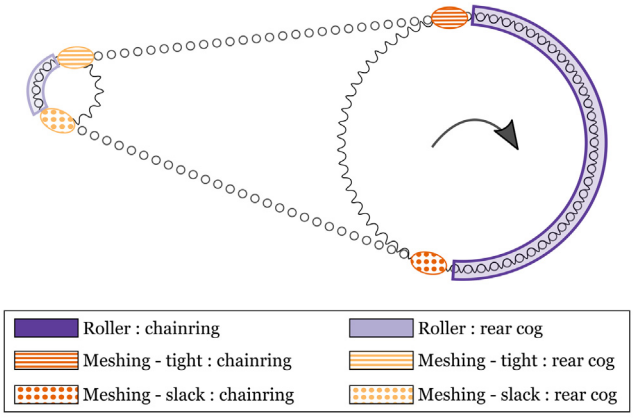

Fig. 18. Location of loss sources.

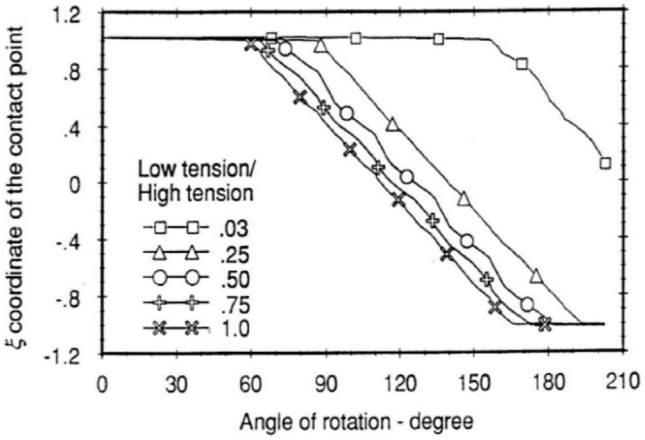

Fig. 20. Evolution of ξ for various T_s/T_t ratio [18].

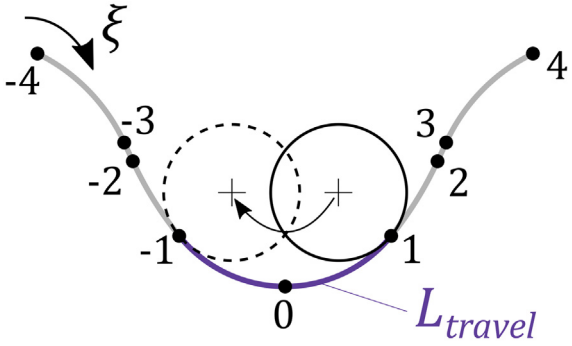

Fig. 19. Definition of ξ for ASA tooth profile [18].

4.2 Frictional motions

During link meshing, the angles of interest are $\alpha_{t,j}$ or $\alpha_{s,j}$, depending on the considered meshing point. Figure 15 shows that each link experiences an articulation angle of α_j during its meshing motion (with j being set to the value corresponding to the appropriate sprocket).

The phenomenon of roller motion has been studied by Kim and Johnson [18] and Troedsson and Vedmar [19]. However, Kim and Johnson based their study on the ASA profile (such as Lodge et al. in [4]) while Troedsson and Vedmar considered a DIN profile. As the tooth profile can have an influence on the roller motion, the results of Kim are used here in agreement with the Lodge's tension model used in Section 2.2.

Kim and Johnson introduced the coordinate ξ, to locate the position of the contact point between each roller and its corresponding tooth profile (Fig. 19). ξ ranges in the interval $[-4, 4]$ and is an integer at the transition points between two distinct curve sections.

In [18] it is shown that, for a wide range of tension ratio T_s/T_t, the rollers tend to go from $\xi = 1$ to $\xi = -1$ (Fig. 20).

Knowing the definition of the ASA tooth profile [11,18], it is, possible to calculate the distance L_{travel}, travelled by the contact point during the rotation of a given sprocket (see Fig. 19).

4.3 Loss calculation

4.3.1 Meshing loss

The meshing phenomenon depends on the type of articulation involved (i.e. pin or bush articulation [4,18,24]). For a pin articulation, friction only occurs at the pin/bush contact while it occurs at both pin/bush and bush/roller contacts for a bush articulation (see Fig. 2). In this study, the differences between pin and bush articulations are neglected [5,6,15] and Coulomb's law of friction is assumed. Therefore, the losses associated with the meshing motion can be estimated with the following expression:

$$W_{mesh} = \mu_{pb} \alpha R_{pin} T \tag{18}$$

with:
- W_{mesh}, the amount of dissipated energy during the meshing of one link at the considered articulation point (Fig. 18).
- μ_{pb}, the friction coefficient for the pin/bush contact.
- $T = T_t$ or T_s, and $\alpha = \alpha_1$ or α_2, depending on the considered meshing point.

4.3.2 Roller loss

When a roller moves along its tooth profile, friction can occur at two contacts, between roller and tooth and between bush and roller (see Fig. 2). As explained above (Sect. 4.2), the distance travelled by the contact point between each roller and its corresponding tooth profile is known. However, the conditions (i.e. sliding or rolling) at both roller/tooth and roller/bush contacts are not determined during this movement.

In order to evaluate the influence of these contact conditions on losses, two extreme cases are considered:
- Pure sliding occurs at the roller/profile contact while pure rolling (i.e. no loss) occurs at bush/roller contact.
- Pure rolling occurs at roller/profile contact and pure sliding at bush/roller contact.

Table 2. Characteristics of the tested drive configurations.

$Z_1\|Z_2$	T_s/T_t	L(mm)	Number of links	Pitch (mm)
60|15	0.5	386	100	12.7
	0.1			
	0.01			
30|15	0.5	389	84	
	0.1			
	0.01			
15|15	0.5	387	76	
	0.1			
	0.01			

Table 3. Chain characteristics.

Pitch (mm)	$\boldsymbol{R_{pin}}$ (mm)	$\boldsymbol{R_{bush}}$ (mm)	$\boldsymbol{R_{roller}}$ (mm)
12.7	1.83	2.591	3.875

Case (b) seems more likely due to the smaller bush radius (compared to roller radius), inducing a larger tangential force for a given torque. However, considering the two extreme cases allows to estimate the result variability with respect to the contact conditions.

For both cases, as a first estimate, each roller is assumed to travel the distance L_{travel} while being subjected to a constant force $\overline{P_j}$. This force is computed as the mean value of P_i for all rollers (and for all transmission positions). Consequently, two values of $\overline{P_j}$ are obtained, one for each sprocket.

Thus, still assuming Coulomb's law of friction, the following equations are used for the calculation of roller losses:

$$\begin{cases} \text{Case (a)} : W_{roller} = \mu_{rp}\overline{P_j}L_{travel} \\ \text{Case (b)} : W_{roller} = \mu_{br}\overline{P_j}\theta_{roller}R_{bush} \end{cases} \quad (19)$$

with:
- W_{roller}, the quantity of energy dissipated by the movement of one roller during its travel within a given sprocket.
- μ_{rp}, the friction coefficient for the roller/profile contact.
- μ_{br}, the friction coefficient for the bush/roller contact.
- $\theta_{roller} = L_{travel}/R_{roller}$, the angle travelled by a roller when rolling over the distance L_{travel} on the tooth flank.
- $\overline{P_j}$, the mean value of P_i for the considered sprocket.

5 Results and discussion

According to Section 4, the proportion of each power loss source is calculated for three different gear and tension ratios for a total of nine cases (Tab. 2).

For the loss computation, the chain dimensions are given Table 3.

The friction angle δ (Fig. 11) is equal to 5° ($0.0873 rad$), corresponding to a friction coefficient of about 0.09 [23]. Moreover, all the friction coefficients are assumed to be identical ($\overline{\mu} = \mu_{pb} = \mu_{rp} = \mu_{rb}$). Therefore, the obtained proportions are independent from this parameter.

The relative contribution, for case (b), of meshing and roller losses are shown in Figure 21. Both contributions are of the same order of magnitude for all the tested configurations (see Fig. C1 for case (a) in Appendix C).

Figure 22 compares the variation induced by the contact conditions (case (a) or (b)). The proportions are calculated for $Z_1|Z_2 = 60|15$ and $T_s/T_t = 0.1$.

The roller losses have a larger contribution for case (a) than for case (b). This is consistent with the longer slip distance for case (a) ($R_{roller} > R_{bush}$). However, the obtained proportions are equivalent in terms of order of magnitude.

It is also possible to further distinguish the different contributions. The meshing losses can be divided between the four meshing points and the roller motion losses can be split between the contribution of the chainring and the rear cog (Fig. 18). The obtained proportions are presented in Table 4 and Figure 23. (For case (b), $Z_1|Z_2 = 60|15$ and $T_s/T_t = 0.1$.)

For this particular configuration, both the roller motion and the tight meshing point for the rear cog are responsible for most part of the losses (about 76%, Table 4 and Fig. 23). Indeed, the relatively low slack tension leads to smaller loss in the corresponding meshing points (compared to the tight strand contribution). Furthermore, the high number of teeth of the chainring reduces the angle α_1 and the corresponding $\overline{P_1}$ value.

A general outline for chain drives is that, the smaller the number of teeth, the bigger the problems. Indeed, a small number of teeth tends to increase losses, but also polygonal effect and, at a lesser extent, transmission error (i.e. deviation of $\dot{\psi}_{t,2}/\dot{\psi}_{t,1}$ from the mean ratio Z_1/Z_2), which may lead to vibration issues.

As all the losses are directly dependent to the friction coefficient $\overline{\mu}$, it can be used as a fitting parameter to obtain 99% of efficiency for a two sprocket drive (see Introduction). For the considered single speed drive ($Z_1|Z_2 = 60|15$ and $T_s/T_t = 0.1$), 99% of global efficiency is obtained for a value of $\overline{\mu} = 0.05$. This seems low for usual bicycle chain

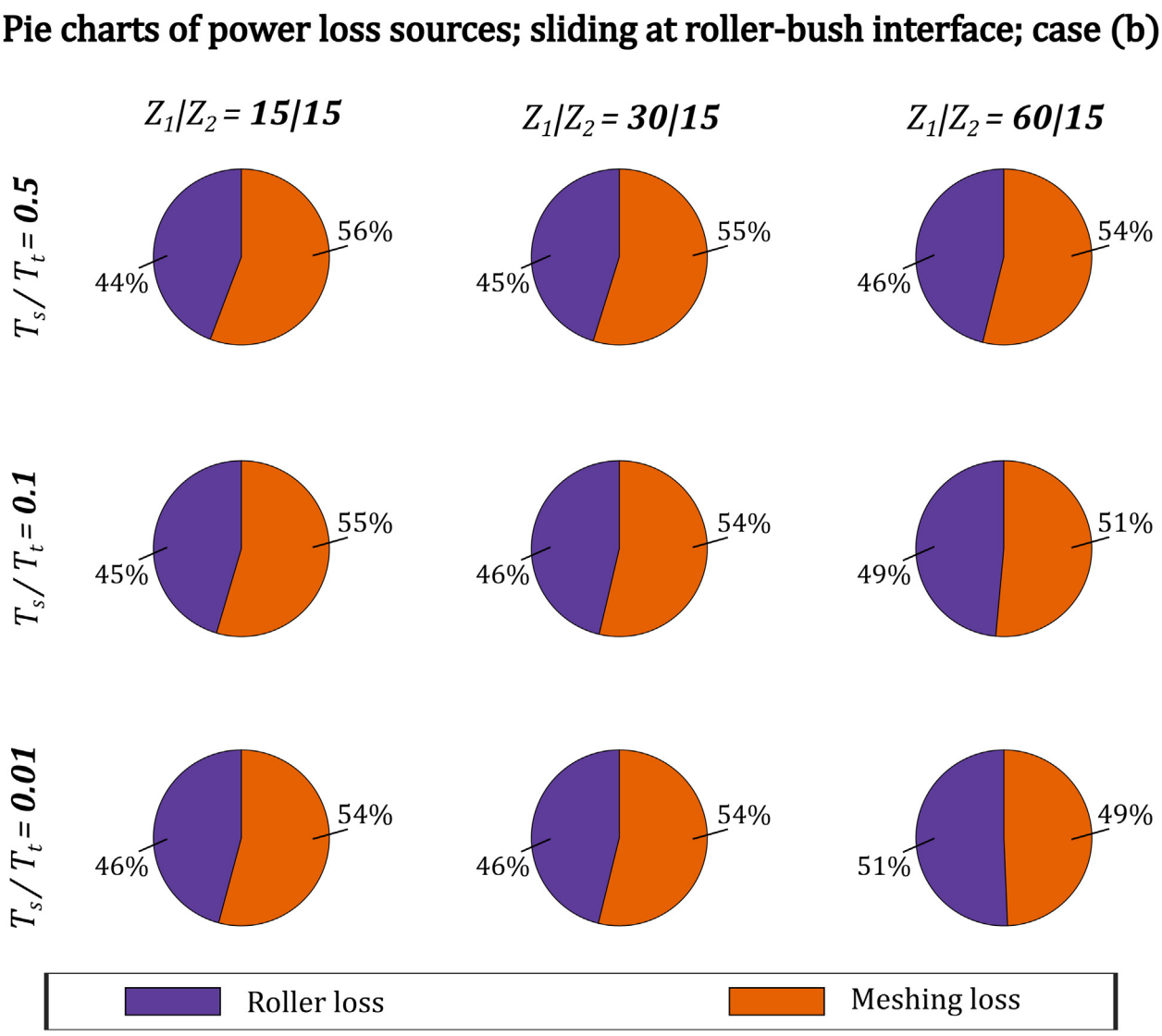

Fig. 21. Pie charts for case (b).

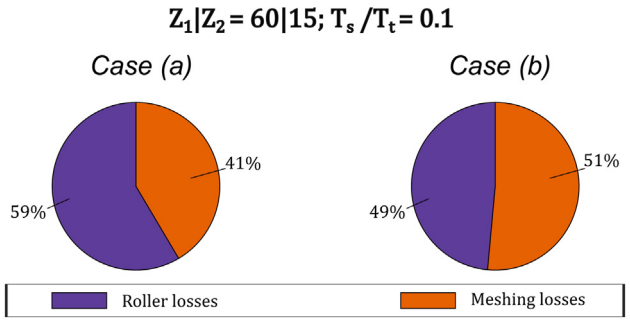

Fig. 22. Comparison between case (a) and (b).

(friction coefficients of about 0.1 are claimed in [25]). Thus, the model probably tends to overestimate the losses. This overestimation could be caused by the assumptions stated in Section 4.3. Mainly, $\overline{P_j}$ is calculated as the mean value of all the P_i while it seems from Figure 20 that most part of the roller motion is performed under the smaller values of contact forces (see Fig. 17).

However, the order of magnitude of $\overline{\mu}$ is still acceptable for the considered application. Therefore, the model can be used for a first loss estimation in chain drives.

Besides, the aim of the model presented in this paper is to compare in a simplified way the magnitude of the losses caused by meshing and roller motion. Therefore, the conclusions based on this study are only valid to give estimates and orders of magnitude. The reality of the phenomena at stake in a real chain articulation is very complex and requires deeper investigations to be computed with more precision.

Furthermore, although Naji and Marshek claimed that their influence on the load distribution should be minimal [22], the deformations of the drive components (mainly link elongation and tooth deflection), neglected in the presented model could have an influence on the global behaviour of the drive. For instance, the elongation of the tight strand

Table 4. Detailed proportion for 60|15; $\boldsymbol{T_s/T_t = 0.1}$; case (b).

Meshing loss	51%	Tight – rear cog	37%
		Tight – chainring	9%
		Slack – rear cog	4%
		Slack – chainring	<1%
Roller loss	49%	Rear cog	39%
		Chainring	10%

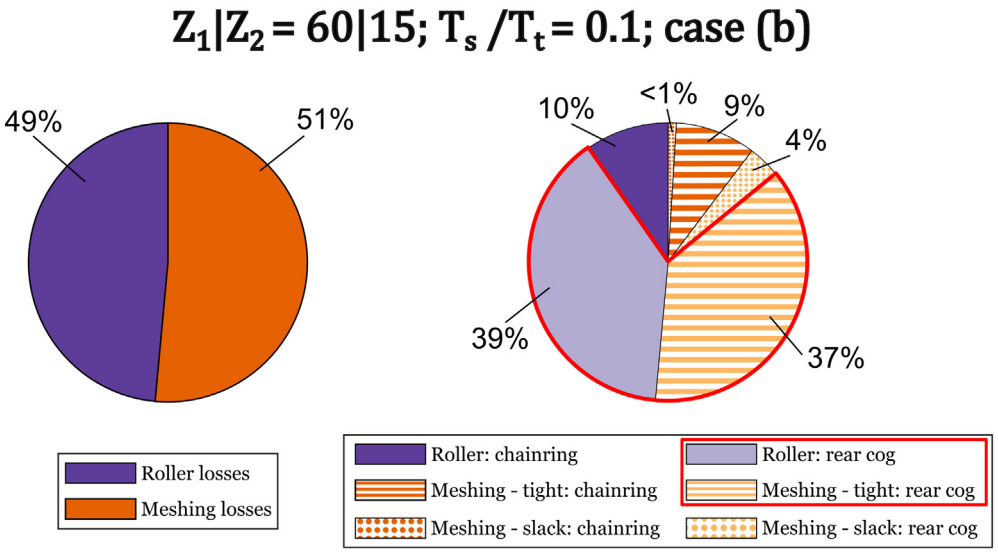

Fig. 23. Split pie chart for 60|15; $T_s/T_t = 0.1$; case (b).

will change the phasing of chainring and rear cog rotations (i.e. relation between $\psi_{t,1}$ and $\psi_{t,2}$).

In this paper, friction is modelled at the scale of the mechanism. Therefore, the study did not focus on the tribological status of the contacts but rather on the global influence of friction on the drive behaviour. Going to the contact scale could exhibit differences between the different involved contacts. For instance, if the roller/sprocket contact is relatively easy to lubricate, the bush/roller and specially the pin/bush contact could be quite difficult to access for lubricant. Therefore, the friction coefficients can differ depending on the contact and this can affect the loss proportions.

6 Conclusion

A model of roller chain drive is presented. Quasi-static evolution and straight chain strands are assumed. This model determines the kinematic evolution as well as the load distribution (in the links and at roller/sprocket contact) throughout the transmission operation. The stated hypotheses are consistent for applications to single speed transmissions. However, the model can be generalised to any chain drive application as long as the assumptions remain valid.

Using Coulomb's law of friction, this model is then used to estimate the contribution of the meshing and roller motions to the global drive efficiency. The meshing articulation angle is deduced from the model results while the roller motion is obtained from previous works. The latter is assumed to be independent from the loading conditions and performed under a constant contact force.

The results show that, for a wide range of gear and tension ratios, the two sources of loss have contributions of similar order of magnitude. Thus, it does not seem justified to neglect one over the other when considering chain drive efficiency.

Based on this statement, the phenomenon of roller motion should be studied in detail and possibilities for optimisation should be investigated. In particular, the distance travelled by each roller depending on the loading conditions should be characterised. A tribological study of the different contacts involved (pin/bush, bush/roller and roller/profile) considering their specific characteristics (lubrication, sliding speed, etc.) would also provide a good estimation of the different friction coefficients. This would help to increase the accuracy of the obtained loss predictions. In addition, this tribological study could help the understanding of the sliding/rolling conditions in the contacts, thus improving the reliability of the associated assumptions.

Conflict of interest

The authors declare that they have no conflict of interest related to this work.

Nomenclature

f [−]	Parameter for the phasing of the chainring and rear cog rotations (related to L) in [21]
L (m)	Distance between the chainring and rear cog axes
L_{travel} (m)	Distance covered by the roller/tooth profile contact point
$n_{s,t}$ [−]	Number of links in a chain strand
n_j [−]	Number of links with both rollers contacting sprocket j
P_i (N)	Contact force between sprocket and roller i
$\overline{P_j}$ (N)	Mean value of P_i for sprocket j (for all rollers and all transmission positions)
p (m)	Chain and sprocket pitch
q_+ [−]	Ratio between T_i and T_{i+1} with positive δ correction
q_- [−]	Ratio between T_i and T_{i+1} with negative δ correction
R_j (m)	Pitch radius of sprocket j
R_{bush} (m)	Outside bush radius
R_{pin} (m)	Outside pin radius
R_{roller} (m)	Outside roller radius
T_i (N)	Tension force into link i
$T_{s,t}$ (N)	Tension force in a chain strand
W_{mesh} (J)	Dissipated energy for a considered meshing motion
W_{roller} (J)	Dissipated energy for a considered roller motion
$x_{s,t,hyp}$ (m)	Length of a chain strand
Z_j [−]	Number of teeth of sprocket j
α_j [rad]	Angular pitch and articulation angle of sprocket j
$\alpha_{s,t,j}$ [rad]	Angle between a chain strand and the closest link with both rollers contacting sprocket j
β [rad]	Tilt angle of the pitch circles common tangent
$\beta_{s,t}$ [rad]	Tilt angle of a chain strand
δ [rad]	Friction angle
θ_{roller} [rad]	Roller rotation angle when rolling a distance of L_{travel}
μ [−]	Friction coefficient for the computation of the friction angle
μ_{pb} [−]	Friction coefficient for the pin/bush contact
μ_{br} [−]	Friction coefficient for the bush/roller contact
μ_{rp} [−]	Friction coefficient for the roller/profile contact
$\overline{\mu}$ [−]	Unique friction coefficient for the loss proportion calculation
ξ [−]	Roller/tooth profile contact point coordinate [18]
ϕ [rad]	$\phi = (35° - 120°/Z) \times (\pi/180)$, pressure angle for seated roller [11]
ϕ_{min} [rad]	$\phi_{min} = (17° - 64°/Z) \times (\pi/180)$, pressure angle for roller climbing the tight side of the tooth profile [11]
$\psi_{s,t,j}$ [rad]	Angle between a strand tip on sprocket $j$and the point of tangential contact
$\dot{\psi}_{t,j}$[rad.s^{-1}]	Time derivative of $\psi_{t,j}$
$\psi_{t,j}$[rad.s^{-1}]	Second time derivative of $\ddot{\psi}_{t,j}$
$\psi_{t,1,init}$ [rad]	Initial value for angle $\psi_{t,1}$
i	Subscript for links and rollers numbering
j	Subscript for sprocket numbering; 1 for the chainring and 2 for the rear cog
s	Subscript for slack strand attributes
t	Subscript for tight strand attributes

Acknowledgements. This work is founded by INSA Lyon and is part of the THPCA^{2024} project supported by ANR (Grant No. ANR-2020-STHP2-000). The authors thank Jérôme CAVORET and Martin BEST for their relevant remarks and ideas during the conception of this studies. The authors would also like to thank Jean-Christophe PERAUD for is support during the study as part of the THPCA^{2024} project.

Appendix A: Solving the equilibrium of an articulation with seated roller

As presented in Figure A1, the $\vec{x}$ axis is defined as $\vec{x} = \vec{T_i}/||\vec{T_i}||$. $\vec{y}$ is then chosen so that the $\vec{z}$ axis of the direct basis based on $\vec{x}$ and $\vec{y}$ is the outgoing normal.

All the forces are considered concurrent at the roller centre (friction torque is neglected). Therefore, the equilibrium is only projected along the $\vec{x}$ and $\vec{y}$ directions.

$$\begin{cases} T_i - P_i \cos(\phi_{eq}) - T_{i+1} \cos(\alpha) = 0 \\ P_i \sin(\phi_{eq}) - T_{i+1} \sin(\alpha) = 0 \end{cases} \tag{A.1}$$

which can be rearranged as

$$\begin{cases} T_{i+1} = T_i \dfrac{\sin(\phi_{eq})}{\sin(\phi_{eq} + \alpha)} \\ P_i = T_i \dfrac{\sin(\alpha)}{\sin(\phi_{eq} + \alpha)} \end{cases} \tag{A.2}$$

The value of ϕ_{eq} can then be set to $\phi \pm \delta$ depending on the side in contact (tight or slack) and on the considered sprocket.

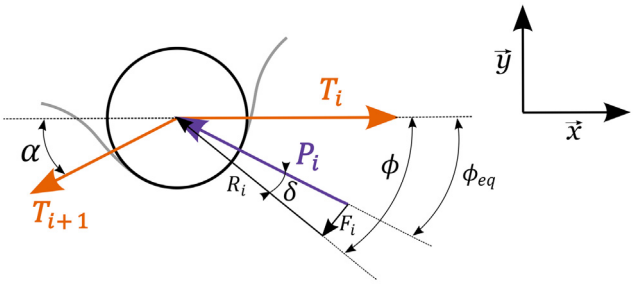

Fig. A1. Articulation equilibrium with $\vec{x}$ and $\vec{y}$ axis.

Appendix B: Comparison with Fuglede et al. [21]

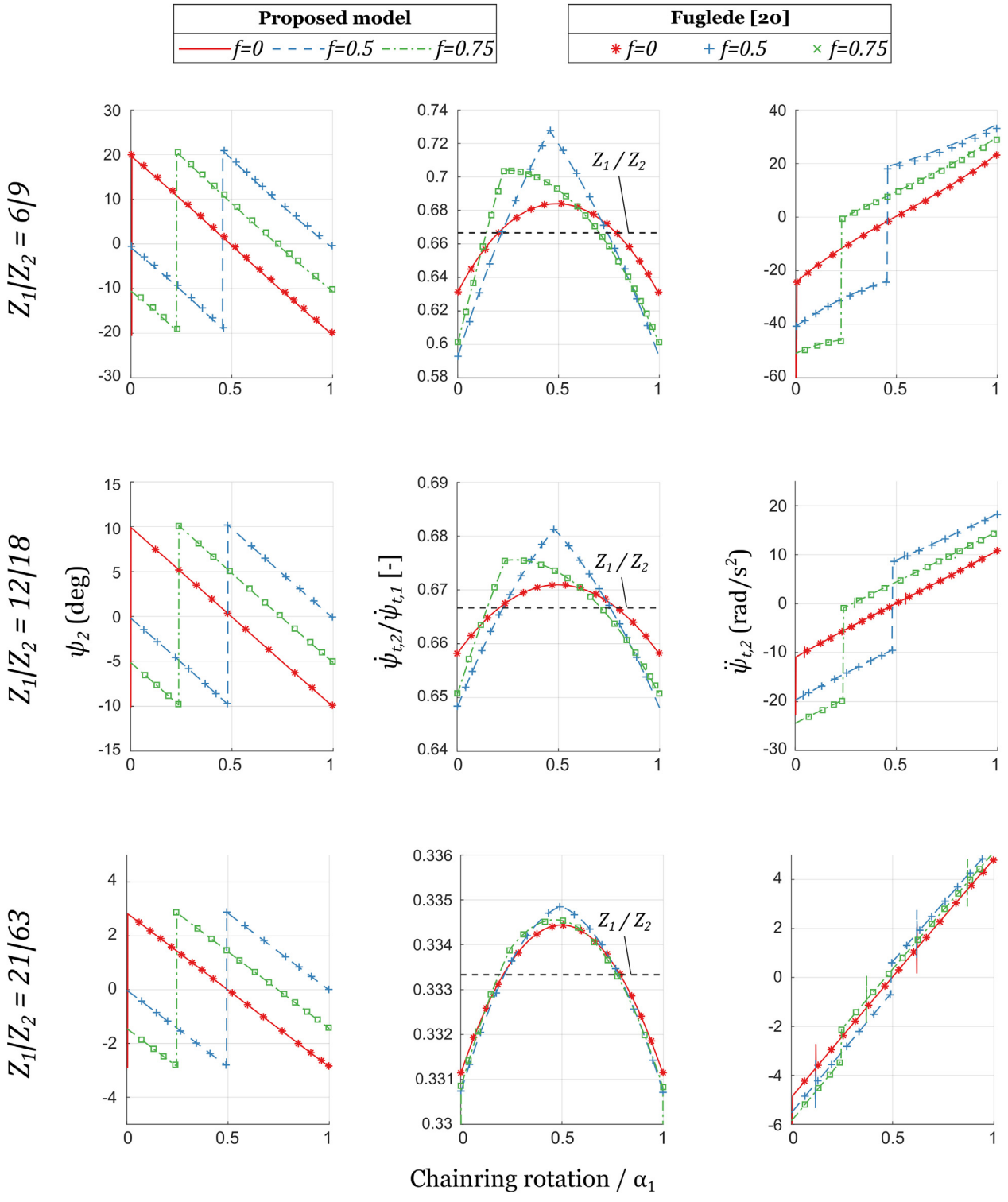

Fig. B1. Chain drive kinematics, comparison with Fuglede et al. [21].

Appendix C: Pie charts for case (a)

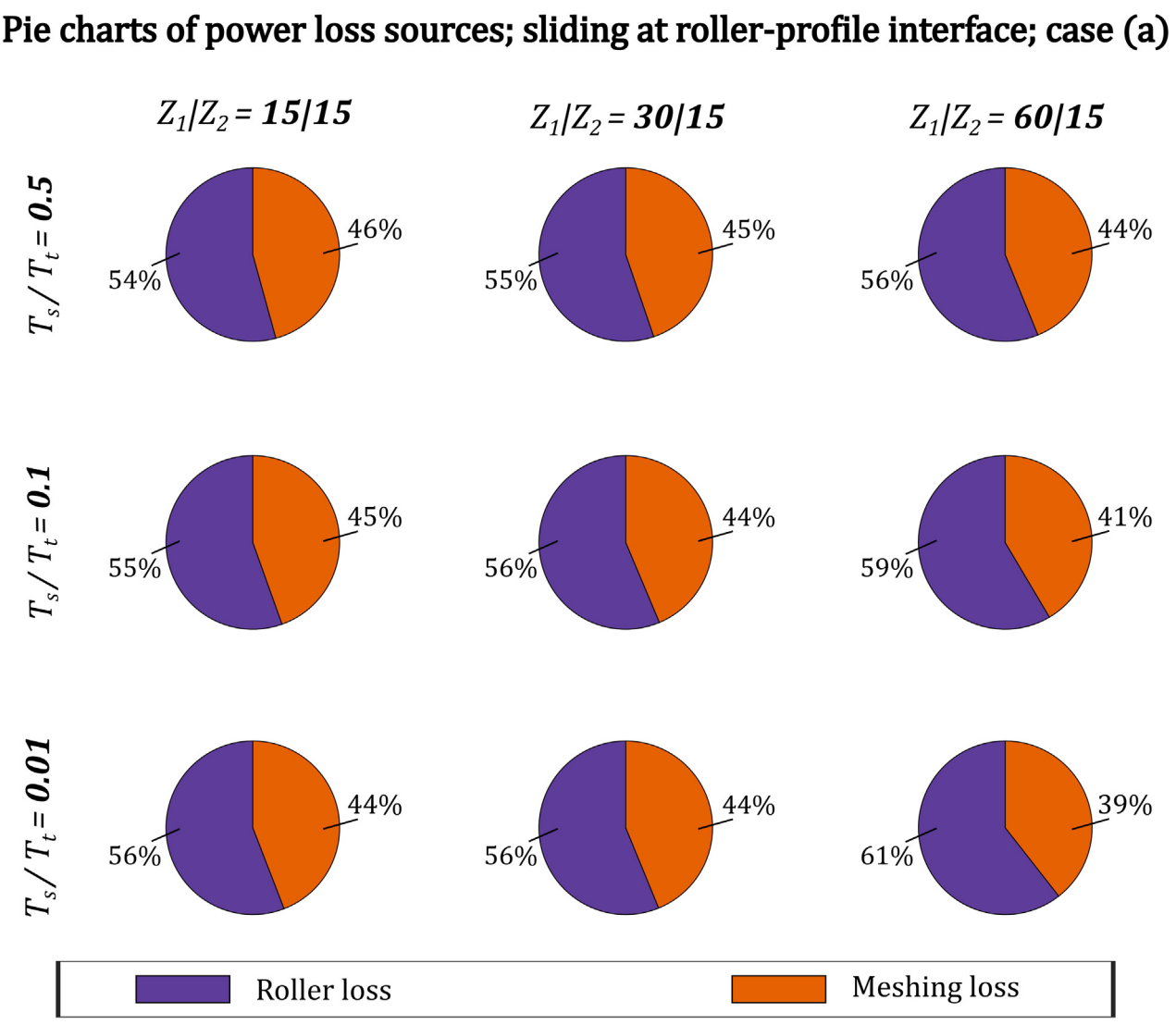

Fig. C1. Pie charts for case (a).

References

[1] R. Stephenson, D. Glennie, J.N. Fawcett, J.M. Hale, A method of measuring the dynamic loads in high-speed timing chains, Proc. Inst. Mech. Eng. Part D **214**, 217–226 (2000), https://doi.org/10.1177/095440700021400211

[2] R. Tandler, N. Bohn, U. Gabbert, E. Woschke, Experimental investigations of the internal friction in automotive bush chain drive systems, Tribol. Int. **140**, 105871 (2019), https://doi.org/10.1016/j.triboint.2019.105871

[3] R. Tandler, N. Bohn, U. Gabbert, E. Woschke, Analytical wear model and its application for the wear simulation in automotive bush chain drive systems, Wear **446–447**, 203193 (2020), https://doi.org/10.1016/j.wear.2020.203193

[4] C.J. Lodge, S.C. Burgess, A model of the tension and transmission efficiency of a bush roller chain, Proc. Inst. Mech. Eng. Part C **216**, 385–394 (2001), https://doi.org/10.1243/0954406021525179

[5] M.D. Kidd, N.E. Loch, R.L. Reuben, Bicycle chain efficiency (Heriot-Watt University, Scotland, 2000)

[6] J.B. Spicer, C.J.K. Richardson, M.J. Ehrlich et al., Effects of frictional loss on bicycle chain drive efficiency, J. Mech. Des. Trans. ASME **123**, 598–605 (2001), https://doi.org/10.1115/1.1412848

[7] N.E. Hollingworth, D.A. Hills, Theoretical efficiency of a cranked link chain drive, Proc. Inst. Mech. Eng. Part C **200**, 375–377 (1986), https://doi.org/10.1243/PIME_PROC_1986_200_141_02

[8] J.B. Spicer, Effects of the nonlinear elastic behavior of bicycle chain on transmission efficiency, J. Appl. Mech. Trans. ASME **80**, 021005 (2013), https://doi.org/https://doi.org/10.1115/1.4007431

[9] S.P. Zhang, T.O. Tak, Efficiency estimation of roller chain power transmission system, Appl. Sci. **10**, 1–13 (2020), https://doi.org/10.3390/app10217729

[10] J.N. Fawcett, S.W. Nicol, Vibration of a roller chain drive operating at constant speed and load, Proc. Inst. Mech. Eng. **194**, 97–101 (1980), https://doi.org/10.1243/PIME_PROC_1980_194_012_02

[11] R.C. Binder, Mechanics of the Roller Chain Drive: Based on Mathematical Studies by R. C. Binder (Prentice-Hall, 1956)

[12] R.A. Sack, Transverse oscillations in travelling strings, Br. J. Appl. Phys. **5**, 224–226 (1954), https://doi.org/10.1088/0508-3443/5/6/307

[13] S. Mahalingam, Transverse vibrations of power transmission chains, Br. J. Appl. Phys. **8**, 145–148 (1957), https://doi.org/10.1088/0508-3443/8/4/303

[14] J.N. Fawcett, S.W. Nicol, Influence of lubrication on tooth-roller impacts in chain drives, Inst. Mech. Eng. Proc. **191**, 271–275 (1977), https://doi.org/10.1243/pime_proc_1977_191_033_02

[15] B. Kohler, E. Sztrygler, Chaînes mécaniques. Tech l'ingénieur Fonct Compos mécaniques base docum (1989)

[16] M.R. Naji, K.M. Marshek, Analysis of roller chain sprocket pressure angles, Mech. Mach. Theory **19**, 197–203(1984), https://doi.org/10.1016/0094-114X(84)90042-9

[17] M.R. Naji, K.M. Marshek, The effects of the pitch difference on the load distribution of a roller chain drive, Mech. Mach. Theory **24**, 351–362 (1989), https://doi.org/10.1016/0094-114X(89)90065-7

[18] M.S. Kim, G.E. Johnson, Mechanics of roller chain-sprocket contact: a general modelling stragegy, in American Society of Mechanical Engineers, Design Engineering Division (Publication) DE (1992), pp. 689–695

[19] I. Troedsson, L. Vedmar, A method to determine the static load distribution in a chain drive, Proc. Inst. Mech. Eng. Part C **215**, 569–579 (2001), https://doi.org/10.1243/0954406011520959

[20] S. Mahalingam, Polygonal action in chain drives, J. Franklin Inst. **265**, 23–28 (1958), https://doi.org/10.1016/0016-0032(58)90665-3

[21] N. Fuglede, J.J. Thomsen, Kinematics of roller chain drives – exact and approximate analysis, Mech. Mach. Theory **100**, 17–32 (2016), https://doi.org/10.1016/j.mechmachtheory.2016.01.009

[22] M.R. Naji, K.M. Marshek, Analysis of sprocket load distribution, Mech. Mach. Theory **18**, 349–356 (1983), https://doi.org/10.1016/0094-114X(83)90130-1

[23] M.R. Naji, K.M. Marshek, Experimental determination of the roller chain load distribution, J. Mech. Des. Trans. ASME **105**, 331–338 (1983), https://doi.org/10.1115/1.3267365

[24] N.E. Hollingworth, D.A. Hills, Forces in a heavy-duty drive chain during articulation, Proc. Inst. Mech. Eng. Part C **200**, 367–374 (1986), https://doi.org/10.1243/PIME_PROC_1986_200_140_02

[25] R. Wragge-Morley, J. Yon, R. Lock et al. A novel pendulum test for measuring roller chain efficiency, Meas. Sci. Technol. 29 (2018). https://doi.org/10.1088/1361-6501/aaa239

Cite this article as: G. Lanaspeze, B. Guilbert, L. Manin, F. Ville, Preliminary modelling of power losses in roller chain drive: application to single speed cycling, Mechanics & Industry **23**, 27 (2022)